NJC

New Journal of Chemistry

An international journal of the chemical sciences

www.rsc.org/njc

Volume 34 | Number 2 | February 2010 | Pages 173–368

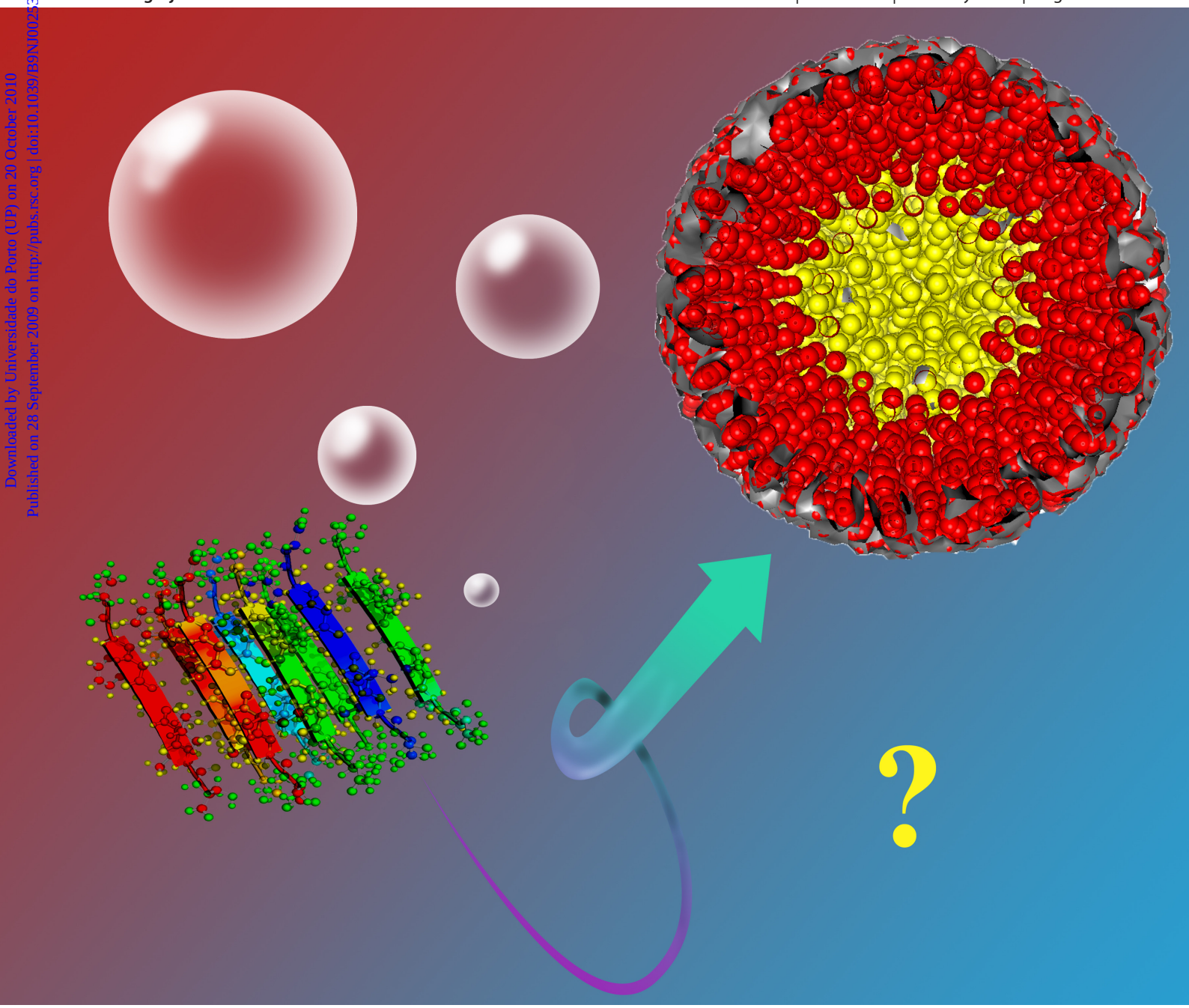

ISSN 1144-0546

RSC Publishing

PAPER

Domenico M. Grasso *et al.*
Are fibril growth and membrane damage linked processes? An experimental and computational study of $IAPP_{12-18}$ and $IAPP_{21-27}$ peptides

1144-0546(2010)34:2;1-Q

Are fibril growth and membrane damage linked processes? An experimental and computational study of $IAPP_{12–18}$ and $IAPP_{21–27}$ peptides

Michele F. M. Sciacca,[a] Matteo Pappalardo,[a] Francesco Attanasio,[b] Danilo Milardi,[b] Carmelo La Rosa[a] and Domenico M. Grasso*[a]

Received (in Gainesville, FL, USA) 10th June 2009, Accepted 18th August 2009
First published as an Advance Article on the web 28th September 2009
DOI: 10.1039/b9nj00253g

Islet amyloid polypeptide (IAPP) is a 37-residue hormone known to deposit as fibrillar aggregates in pancreatic β-cells of patients affected by T2DM. Although it has been proposed that both the fibrillogenic potential and membrane-activity may play a key role in IAPP cytotoxicity, a direct causative relationship between these two properties has not yet been firmly established. More recently, it has been observed that membrane damage may occur independently from fiber formation of IAPP and that these properties may be encoded by different sequences of IAPP. To further check this hypothesis, the membrane-activity and aggregation properties of the two neutral segments LANFLVH ($IAPP_{12–18}$) and NNFGAIL ($IAPP_{21–27}$), that recent theoretical studies have reported to possess the highest and the lowest fibrillogenic potential respectively, have been studied by means of a combined experimental and computational approach. The whole of the results demonstrate that if neutral peptides and lipids are employed, the most fibrillogenic peptide has the lowest membrane damaging effect and *vice versa*. These findings are expected to contribute to our rational understanding of the factors involved in the formation of amyloidosis and in the mechanisms of peptide-induced membrane damage.

Introduction

A growing number of polypeptides and proteins have been shown to form partially structured deposits known as "amyloids" that are thought to contribute to the pathogenesis of a number of diseases, named "Protein Conformational Diseases" (PCDs).[1–4] An important example of these polypeptides is the islet amyloid polypeptide (IAPP), a 37 amino acid residues peptide present in pancreatic β-cell secretory granules and co-secreted with insulin. In type 2 diabetes mellitus (T2DM), IAPP aggregates *in vivo* in the islet extracellular space to form β-sheet rich fibrillar amyloid deposits which are known to be toxic to β-cells.[5–8] *In vitro*, depending on the experimental conditions, IAPP precipitates from aqueous solutions as amorphous aggregates or converts to β-sheet rich structures often accompanied by amyloid formation.[9–11] A possible mechanism of IAPP toxicity is believed to be related to the IAPP-induced disruption of natural lipid membranes.[12–14] Recent studies on the non-cytotoxic rat variant of IAPP (rIAPP) have provided significant hints on this respect since as rats do not develop T2DM.[15,16] Although the nature of the toxic species is still debated, soluble oligomers of human IAPP (hIAPP) have been shown to kill β-cells by binding to and damaging the cellular membrane.[10,17,18] Other amyloidogenic peptides such as amyloid-β (Aβ), α-synuclein, and polyglutamine have also been found to cause cell death by a similar mechanism[19] and therefore, there is considerable interest in investigating the interaction of such amyloidogenic peptides with phospholipid membranes. Dissecting the properties of different IAPP sequences is believed to be an effective strategy to identify the molecular features driving amyloid fibril formation, membrane activity and, eventually, toxicity. This approach has proven to be effective in the development of inhibitory agents for the Aβ peptide associated with Alzheimer's disease.[20–22] In this light, a single amyloidogenic region spanning residues 20–29 (NFGAIL) has been proposed to be a critical domain in fibril formation of IAPP.[23–27] The decapeptide $hIAPP_{20–29}$ has been found to form fibrils in a antiparallel β-sheet conformation and in a morphology that is similar to the fibrils formed by the complete hIAPP sequence.[28–30] In addition, the N-terminal half of IAPP (residues 1–20) has been shown to have a number of unique features that may affect folding and/or aggregation. These observations indicate that peptides corresponding to residues 8–20, 10–19, 20–29, 30–37 and 8–37 of human amylin all form amyloids.[31–35] However, in contrast to fragments from the 20–29 domains, the peptides from the 8–20 region are not known to be toxic.[36] In an attempt to rationalize the physico-chemical principles of amyloidogenesis and understand the specific role of sequences in driving the behaviour of the entire protein, several theoretical models able to predict protein aggregation propensities from primary structures have been proposed.[37,38] In particular a novel approach to structurally characterize the propensity towards ordered β-aggregation of amyloid polypeptides has been recently applied to the hIAPP sequence.[39,40] The β-aggregation profile of hIAPP 1–37 confirmed, on one hand the high aggregation

[a] *Dipartimento di Scienze Chimiche Università di Catania, Viale Andrea Doria 6, 95125 Catania, Italy. E-mail: dgrasso@unict.it; Fax: ++3995580138; Tel: ++39957385204*
[b] *Istituto CNR di Biostrutture e Bioimmagini-Sezione di Catania, Viale Andrea Doria 6, 95125 Catania, Italy*

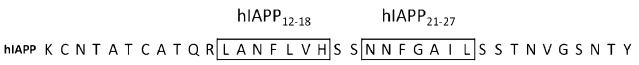

Fig. 1 Amino acid sequence of human IAPP. The two fragments that are used in this study are closed in boxes.

propensity of the region encompassing residues 8–20 (and in particular of the segment 12–18), but on the other hand, indicated a second aggregation hot-spot located in a region (residues 28–30) which is different from the sequence 20–29 that the literature reports as highly fibrillogenic. On the contrary, the above approach has identified the heptapeptide NNFGAIL (residues 21–27) as one of the less aggregation-prone regions of the whole hIAPP sequence.[41]

In order to contribute to shed light on these debated issues, we used differential scanning calorimetry (DSC), membrane-leakage experiments, Thioflavin T binding, and Congo Red staining assays to examine the membrane activity towards zwitterionic lipid bilayers constituted by 1,2-dimyristoyl-*sn*-glycero-3-phosphocholine (DMPC) and the amyloid fibril formation of the two heptapeptides LANFLVH ($hIAPP_{12–18}$) and NNFGAIL ($hIAPP_{21–27}$) (Fig. 1).

Experimental data were paralleled by molecular dynamics simulations in both aqueous and membrane-like environments. Our studies revealed that $hIAPP_{21–27}$ has a propensity to self-assemble into amorphous aggregates which effectively interact with zwitterionic membranes by a poration mechanism. On the contrary, $hIAPP_{12–18}$ rapidly formed amyloid-like aggregates, which did not interact with model membranes. Our findings reconcile with recent reports showing that membrane damage and fibril formation are not directly correlated.

Experimental

Chemicals

The N-acetylated and C-amidated fragments of human amylin, $hIAPP_{21–27}$ and $hIAPP_{12–18}$ were purchased from Genscript corporation with a purity of ≈98%; 1,2-dimyristoyl-*sn*-glycero-3-phosphocholine (DMPC) was purchased from Avanti Polar Lipids, with a purity of ≈98% and used without further purification; 1,1,1,3,3,3-hexafluoro-2-propanol (HFIP), 6-carboxyfluorescein, Thioflavin T (ThT), Congo Red and all salts used for buffer solution preparation were purchased from Sigma–Aldrich, with a purity, at least, of 99%. Before use, peptides were dissolved in HFIP (1.5 mg ml^{-1}) to break up any preformed aggregates present in the solution. Aliquots of the peptide stock solution were rotoevaporated under a gentle nitrogen flow for more than 1 h and then at less than 1 mtorr vacuum for 2 h to completely remove HFIP leaving a transparent film of peptide on the internal surface of the tube: next, it was dissolved in the buffer or, alternatively added to lipid dispersions up to the desired lipid/peptide molar ratio.

Preparation of model membranes

Model membranes were prepared as described elsewhere.[42] Briefly, solutions of DMPC, in $CHCl_3$ were dried under a nitrogen flow and evaporated under high vacuum to dryness in round-bottomed flasks. The resulting lipid film was hydrated with an appropriate volume of phosphate buffer (10 mM, pH = 7.4) and dispersed by vigorous stirring in a water bath set at 4 °C above the gel-liquid crystal transition temperature of the membrane. Control experiments carried out in buffers, with the ionic strength adjusted to 100 mM by adding NaCl, did not reveal any difference in the results. The final nominal concentration of the lipid was 200 μM. In order to obtain large unilamellar vesicles (LUVs), the multilamellar vesicles were extruded through polycarbonate filters (pore size ≈ 100 nm) (Nuclepore, Pleasanton, CA) mounted in a mini-extruder (Avestin Inc.) fitted with two 0.5 ml Hamilton gastight syringes (Hamilton, Reno, NV). Usually we subjected samples to 23 passes through two filters in tandem as recommended elsewhere.[43] An odd number of passages were performed to avoid contamination of the sample by vesicles which might not have passed through the filter.

ThT Fluorescence assays

Fluorescence was monitored as a function of time in a 1 cm path length quartz cuvette by using a Varian Cary Eclipse spectrofluorimeter. Two identical stock solutions of the $hIAPP_{21–27}$ and $hIAPP_{12–18}$ were prepared by dissolving each peptide in 100% HFIP (1.5 mg ml^{-1}). Experiments were performed by adding 10 μl of the peptide stock solution into a glass tube. Then, HFIP was removed by a nitrogen stream followed by a vacuum drying for 1 h. The resulting peptide film was then hydrated with 2 ml of phosphate buffer (10 mM, pH 7.4) containing ThT. In the final solutions the concentrations of ThT and of the peptide were 20 and 10 μM, respectively. In ThT assays in the presence of membranes, the dry peptide film was hydrated with 2 ml of 200 μM lipid dispersion buffered at pH 7.4 containing ThT. All other experimental condition were unchanged. All buffer solutions were filtered by using a 0.2 μm filter. The measurements were carried out by using, as a control, the fluorescence *vs.* time curves of ThT solutions without the peptide. The excitation and emission wavelengths were 440 and 481 nm, respectively. Excitation and emission slits values were maintained at 5 and 10 nm, respectively. Spectra were recorded at 10 min intervals for about 24 h, and all measurements were replicated three times. The measurements were carried out in a thermostated room at 27 °C.

Congo Red staining

Congo Red birefringence of the aggregates under cross polarizer was evaluated by an optical Zeiss Axioplan polarizing microscope equipped with a digital camera. Samples were prepared by adding 1 μl of a hydroalcoholic solution of Congo Red to 3 μl of buffer solutions of the peptide. Glass slices so prepared were dried in air for 6 h. Images were acquired after 20 h under bright-field illumination and then between crossed polars at 50× magnification in order to evaluate the presence of amyloid fibrils. The measurements were carried out in a thermostated room at 27 °C.

Membrane leakage experiments

Membranes leakage experiments were carried out by using 6-carboxyfluorescein-filled LUVs of DMPC (200 μM). Dye-filled DMPC LUVs were prepared by hydrating the dry

lipid film with the buffer solution containing 6-carboxyfluorescein (0.1 M) according to the procedure described above. After the extrusion, LUVs were dialyzed overnight at $T = 20$ °C through a membrane with a cut-off of 2000 Da in order to eliminate the dye not encapsulated into LUVs. Leakage experiments were started by adding an aliquot of peptide stock solution to an empty glass tube. Next, organic solvent was evaporated by using a gentle stream of dry nitrogen followed by vacuum desiccation for 1 h. The resulting peptide film was then dissolved into dye-filled DMPC LUVs (10 μM). Membrane damage was quantified by detecting the increment of fluorescence emission intensity of 6-carboxyfluorescein due to its dilution (dequenching) in buffer as consequence of the membrane leakage. All spectra were corrected by subtracting a baseline obtained as the signal detected prior to the addition of the peptide solution. The excitation and emission wavelength was 490 and 515 nm, respectively. Excitation and emission slits were maintained at 5 and 10 nm, respectively. Spectra were recorded at 30 min intervals for 24 h. All measurements are an average of three replicated experiments. The maximum leakage at the end of each measurement was determined by adding 2 μl of 10% Triton X-100 to a final concentration of 0.1% (vol/vol). The release percentage of the fluorescent dye (membrane leakage) was calculated according to the equation: %release $= (I - I_0)/(I_{100} - I_0)$, where I is the fluorescence intensity at 515 nm of sample, I_0 is the fluorescence at 515 nm in absence of fragments and I_{100} is the fluorescence intensity after the addition of Triton X-100. The measurements were carried out in a thermostated room at 27 °C.

Differential scanning calorimetry (DSC)

DSC runs of DMPC LUVs were carried out on a VP-DSC (MicroCal) apparatus. All the lipid samples were degassed by vacuum and then heated from 10 to 50 °C at a scan rate of 1 °C min^{-1}. Preliminary trials have shown that a 10 mM phosphate buffer pH = 7.4 solution in which peptide and lipid concentrations were 10 and 200 μM, respectively, provided an optimal balance between stability of lipid vesicles and solubility of peptides. Furthermore, it should be mentioned that this lipid : peptide ratio (20 : 1) is largely adopted in DSC experiments of peptide-induced membrane perturbation[16] and represents the better compromise between sensitivity and biological significance of the experiments. An extra external pressure of about 2 bar was applied on the solution to prevent the formation of bubbles during heating. The buffer solution without the sample was used as the reference cell. Heat capacity curves (C_p), were obtained by subtracting the buffer–buffer baseline from raw DSC data. All DSC runs were performed immediately after the preparation of samples, and after 20 h, in order to observe if kinetic effects are present. The results of DSC experiments were the average of three different scans.

Molecular dynamics

Constant temperature molecular dynamics (CT-MD) simulations of N-acetylated and C-amidated $hIAPP_{12-18}$ and $hIAPP_{21-27}$ were performed with the program CHARMM33.[44–46] All peptide systems were modeled by explicitly considering all heavy atoms and the polar hydrogen atoms bound to nitrogen and oxygen. The CHARMM 19 potential function was adopted and default cut-offs for long-range interactions were used, *i.e.* a shift function[37] of 1 Å was employed with a cut-off at 7.5 Å for both the electrostatic and van der Waals terms. Langevin dynamics with a friction value of 0.15 ps^{-1} were used. This friction coefficient is much smaller than that of water (43 ps^{-1} at 330 K, computed as $3\pi\eta d/m$,[38] where η is the viscosity of water at 330 K, and d and m are the effective diameter, *i.e.*, 2.8 Å, and mass of a water molecule, respectively) to allow for sufficient sampling within the time scale (ns) of simulations. It has been demonstrated that the small value of friction adopted does not influence the thermodynamic properties of the system, thus ruling out the possibility of kinetic traps along the aggregation pathway.[38] The implicit solvent model EEF1 was adopted in order to simulate water solvent.[47–49] The DMPC membrane was modeled by use of the implicit solvent model IMM1 which is an extension of EEF1 for modeling proteins in a membrane-like environment.[49] In this model the hydrocarbon core of a DMPC membrane is simply defined as a plane with a thickness of 23.1 Å embedded in a medium with water-like properties. The SHAKE algorithm[44] was used to fix the length of the covalent bonds involving hydrogen atoms, which allows an integration time step of 2 fs. Furthermore, the non-bonded interactions were updated every 10 dynamics steps and the coordinate frames were saved every 20 ps. A 20 ns implicit water MD simulation was performed on each single heptapeptide at $T = 300$ K to equilibrate the monomer. For each heptapeptide, three replicas of the equilibrated monomer were used to simulate aggregation in water and in a membrane-like environment. Control simulations carried out with 11 replicas of the peptides $IAPP_{12-18}$ did not show any significant variations in the results but required very high computational resources.[38] In the initial positions there were neither inter- or intra-molecular contacts, *i.e.* the three peptides were completely unfolded and not interacting in space. All simulations were started from random positions, orientations and conformation of the peptide copies. When the implicit membrane was introduced, the initial position of the mass center of one heptapeptide was chosen in the center of the bilayer; the mass centers of the other two replicas were located 20 Å far away the membrane surface on the two opposite sides of the membrane. The final trimeric assembly was simulated in a cubic box of 186 Å side and re-equilibrated for 20 ns at 300 K. Next, productive MD simulations were carried out at 300 K for overall 2 μs. Implicit membrane MD simulations were paralleled by simulations in water in which all the other parameters were not changed. Here, the nematic order parameter $\bar{P}_2$ was considered to monitor the aggregation process, as described elsewhere.[38] This order parameter is widely used to study the properties of anisotropic fluids[41] and is defined as:

$$\bar{P}_2 = \frac{1}{N}\sum_{i=1}^{N}\frac{3}{2}(\vec{z}_1 \times \vec{d})^2 - \frac{1}{2}$$

where $\vec{d}$ (the director) is a unit vector defining the preferred direction of alignment, $\vec{z}_i$ are the molecular unit vectors linking the peptide's N- and C-termini and N is the number of

molecules in the simulation box, *i.e.* three in the present study. The order parameter $\bar{P}_2$ describes the orientational order of the system and discriminates between ordered and disordered conformations. $\bar{P}_2$ values close to the unity represent highly ordered aggregates while values close to 0.5 represent disordered systems.

Results

Interaction of hIAPP$_{12–18}$ and hIAPP$_{21–27}$ with DMPC membranes determined by differential scanning calorimetry

It is widely acknowledged that DSC is an important tool to investigate the peptide-induced perturbation of lipid bilayers:[40,50] in fact the heat-capacity (C_p) changes concerning the main transition of lipid/peptide systems may help to clarify not only the effects of the presence of the peptide on the physical state of the membrane, but also the topological arrangement of the peptide inserted into a lipid matrix. Indeed, the enthalpy change (ΔH) observed during the lipid main transition is mainly ascribable to the packing efficiency of the hydrocarbon tails.[51] The peptide-induced decrease of the transition enthalpy of the bilayer may thus be related to the extent of the interaction between guest molecules and the hydrocarbon core of lipid membranes. Moreover, the temperature at which the main transition occurs, T_m, is more sensitive to interactions involving the lipid head groups, and changes when the membrane surface is involved in the interaction with the guest peptide.[40,51] Fig. 2 shows C_p profiles of large unilamellar vesicles (LUVs) constituted by DMPC/hIAPP21-27 (molar ratio 20 : 1, dashed lines) and DMPC/hIAPP$_{12–18}$ (molar ratio 20 : 1, dotted lines), compared with C_p profile of pure DMPC (solid line). In order to evidence possible kinetic effects, DSC runs of the lipid/peptide mixtures were performed immediately after the addition of the peptide to LUVs (Fig. 2; upper panel), and repeated after 20 h (Fig. 2; lower panel). All the relative calorimetric data are collected in Table 1.

The effect of the peptides on the phase behavior of DMPC LUVs immediately after its addition to the lipid dispersion (t = 0 h) is evidenced by a small decrease of both enthalpy and temperature of the main transition. DSC runs repeated after 20 h on the same samples demonstrated that the peptide-induced membrane interaction is time-dependent: in particular, the enthalpy change associated with the thermal transition of DMPC LUVs incubated for 20 h with hIAPP$_{21–27}$ was lower than samples scanned immediately after peptide addition. The peptide-induced decrease of both T_m and ΔH coupled with the decrease of the sharpness of the DSC curve is ascribable to the insertion of the peptide into the hydrocarbon core of the bilayer.[52] Conversely, the interaction of hIAPP$_{12–18}$ with DMPC LUVs induced an appreciable decrease in T_m and only weak lowering of ΔH. These effects have been shown to be time-independent because the DSC curve relative to the lipid bilayer incubated for 20 h with hIAPP$_{12–18}$ is similar to the peak recorded by scanning a freshly prepared lipid/peptide mixture. These findings reconcile with a scenario in which hIAPP$_{12–18}$ lies preferentially on the surface of the membrane and does not penetrate into the lipid bilayer.

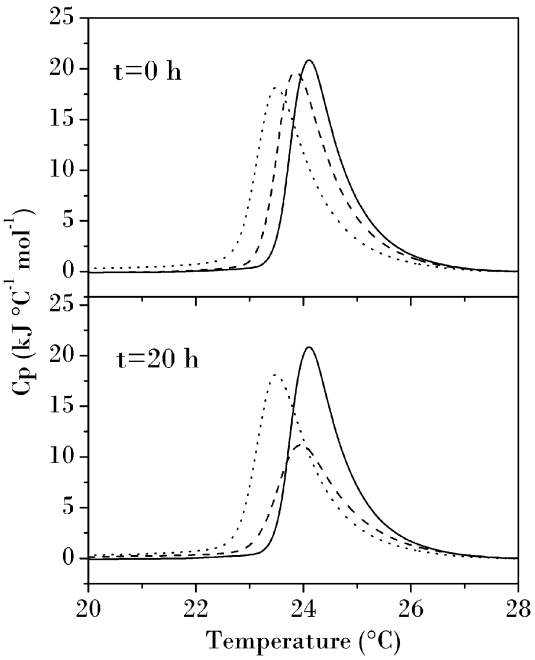

Fig. 2 Heat-capacity profiles (C_p) of LUVs of 20 : 1 DMPC/hIAPP$_{12–18}$ (dotted line) and DMPC/hIAPP$_{21–27}$ (dashed line) obtained immediately after peptide addition to the lipid dispersion (upper panel) and after 20 h of incubation (lower panel). The C_p profile of pure DMPC LUVs (solid line) is also reported in both panels for comparison.

Table 1 Calorimetric parameters ΔH and T_m relative to the main transition of different peptide/lipid LUVs systems at different times of peptide incubation prepared as reported in the Experimental section. The reported values are as the mean of three repeated experiments. Standard deviations are reported in parentheses

Lipid/peptide system	Incubation time, t/h	T_m/°C	ΔH/kJ mol^{-1}
DMPC		24.1 (0.1)	27.2 (1.4)
DMPC + hIAPP$_{21–27}$	0	23.9 (0.1)	25.8 (1.2)
DMPC + hIAPP$_{21–27}$	20	24.0 (0.1)	18.7 (0.9)
DMPC + hIAPP$_{12–18}$	0	22.3 (0.1)	25.1 (1.3)
DMPC + hIAPP$_{12–18}$	20	22.5 (0.1)	25.0 (1.3)

Membrane leakage induced by hIAPP$_{12–18}$ and hIAPP$_{21–27}$

In order to evidence the peptide-induced membrane damage the release of the fluorescent dye, 6-carboxyfluorescein, from DMPC LUVs (Fig. 3) was measured, after incubation of peptide, as a function of time. Fig. 3 shows that hIAPP$_{12–18}$ did not cause appreciable dye release from DMPC vesicles; conversely, hIAPP$_{21–27}$ induced a time-dependent dye release. Moreover, the maximum extent of membrane leakage occurs about 20 h after the addition of hIAPP$_{21–27}$, in agreement with DSC data. The average midpoint ($t_{0.5}$ = 424.15 min) of the experimental curve sigmoidal transition was obtained by fitting the average curve to a standard sigmoidal function (Fig. 3, solid line).

Thioflavine-T (ThT) assays of hIAPP$_{12–18}$ and hIAPP$_{21–27}$ fibril growth in buffer and membranes

Fig. 4 shows the results of ThT-fluorescence assays in presence of hIAPP$_{12–18}$ (open squares) and hIAPP$_{21–27}$ (open circles).

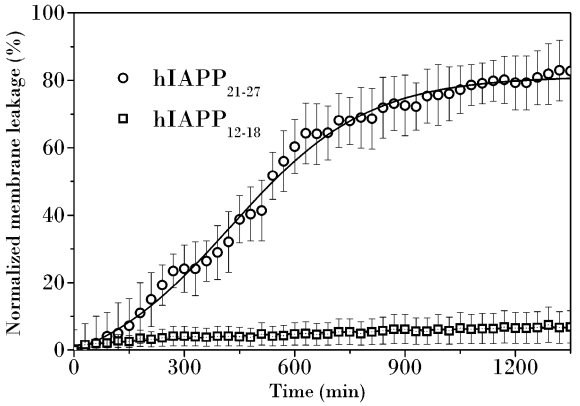

Fig. 3 Normalized membrane leakage *vs.* time measured after the addition of $hIAPP_{12–18}$ (open squares) and $hIAPP_{21–27}$ (open circles) at concentration of 10 μM to dye-filled DMPC LUVs (200 μM lipids). Each point represents the average of three independent experiments performed of freshly prepared peptide solutions. The error bars indicate the standard deviations. Solid lines were obtained by fitting the average curve with a sigmoidal function.

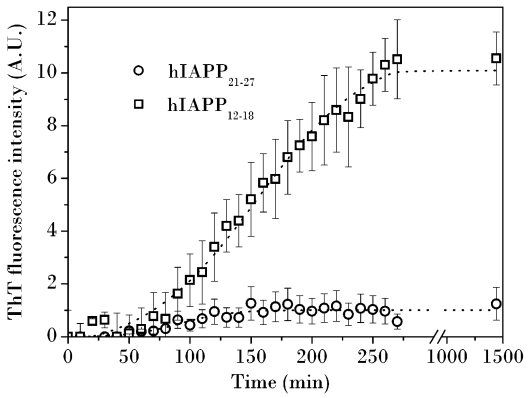

Fig. 4 ThT fluorescence emission profiles *vs.* time of $hIAPP_{12–18}$ (open squares) and $hIAPP_{21–27}$ (open circles) in buffer solution. ThT fluorescence was measured as an average of three independent experiments of freshly prepared peptide solutions and monitored *vs.* time. Dotted lines were obtained by fitting the average curves sigmoidal functions. Experimental conditions are reported in the text.

Whilst the peptide $hIAPP_{21–27}$ did not induce any ThT-fluorescence emission even 20 h after ThT addition to a freshly prepared peptide solution, the $hIAPP_{12–18}$, after a lag phase of 70 min, exhibited a sigmoidal growth of ThT fluorescence as a consequence of fibril-like aggregate formation. If one compares membrane leakage experiments with ThT fluorescence data, one may argue that $hIAPP_{12–18}$ has a remarkable propensity to aggregate in amyloid-like structures, but does not cause membrane damage; conversely, $hIAPP_{21–27}$ that does not exhibit any tendency to aggregate, causes time-dependent membrane damage, and changes in its thermotropic phase behavior.

In the presence of zwitterionic membranes (Fig. 5), $hIAPP_{21–27}$ did not exhibit any propensity to form amyloid fibrils, analogously to what was observed in water. In the same experimental conditions $hIAPP_{12–18}$ did form fibrils, but less rapidly than in water; this suggests that the presence of neutral membranes can only modulate the kinetics of the fibril growth. This is not unexpected because of the low tendency of $hIAPP_{12–18}$ to interact with natural membranes.

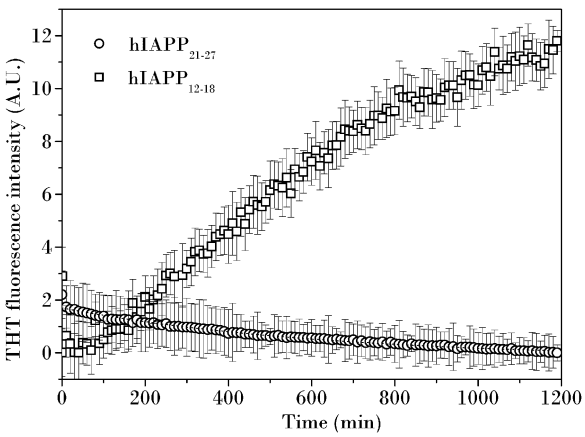

Fig. 5 ThT fluorescence emission profiles of $hIAPP_{12–18}$ (open squares) and $hIAPP_{21–27}$ (open circles) obtained in the presence of DMPC LUVs (200 μM).

Congo Red staining and polarized light microscopy

The amyloid-like structures of the peptide aggregates were also characterized by observing their optical anisotropy after treatment with a Congo Red ethanol solution. Fig. 6 reports some representative images in normal (panel A) and in polarized (panel B) light of $hIAPP_{12–18}$ after 20 h: the observed yellow–green birefringence confirmed that $hIAPP_{12–18}$ is able to form amyloid-like fibrils. Panels C and D show images of the $hIAPP_{21–27}$ aggregates obtained in the same experimental conditions, showing that this fragment cannot form fibrils, in accordance with ThT assays.

Molecular dynamics (MD) simulation of $hIAPP_{12–18}$ and $hIAPP_{21–27}$ aggregation in water and in DMPC membranes

Molecular dynamics simulations of the early stages of peptide aggregation in water and in membrane-like environments are expected to provide complementary information to the experimental results describing lipid–peptide interactions. In particular, the morphology of the aggregates (ordered or amorphous) and the extent of insertion into the lipid matrix may provide fundamental clues concerning the nature of the lipid–peptide interactions. To this aim we have simulated the self-assembly of a trimeric ensemble of $hIAPP_{12–18}$ and, alternatively, of $hIAPP_{21–27}$, either in water and in model membranes. Considering that extended simulations of large systems in explicit solvents (of the order of microseconds) are not easily accessible, we have chosen to describe the environment implicitly using simulation protocols and descriptors largely tested in the literature (see Materials and methods section). In particular MD simulations, were mainly focused on the propensity of $hIAPP_{12–18}$ and $hIAPP_{21–27}$ to form ordered aggregates in water and in membranes, by monitoring the nematic order parameter $\bar{P}_2$ calculated from the analysis of the frames over 2 μs of MD simulations. Fig. 7 (left panel, dashed curve) evidences that in water, $hIAPP_{12–18}$ has a high propensity to self-assemble into highly ordered aggregates ($P_2 = 0.82$), in agreement with previously reported data.[38] However, a small

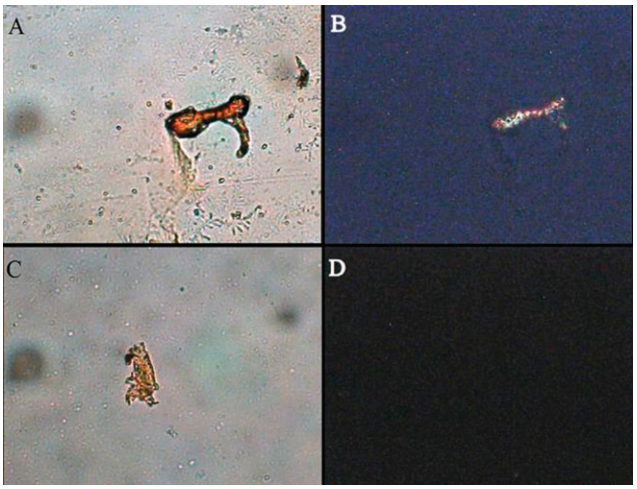

Fig. 6 Optical images of $hIAPP_{12–18}$ aggregates treated with Congo Red and observed in normal (A) and polarized (B) light. In parallel, the images obtained for $hIAPP_{21–27}$ aggregates (C) and (D) are also reported.

shoulder centered at $P_2 = 0.46$ indicates the persistence of a small percentage of amorphous aggregates, which may be ascribed to an equilibrium existing between ordered and disordered aggregates. A parallel set of simulations carried out in implicit membrane shows a sharp peak centered at $P_2 = 0.48$ suggesting that only disordered aggregated configurations are accessible by $hIAPP_{12–18}$ in a membrane-like environment (solid line). Conversely, the self-assembling of $hIAPP_{21–27}$ in water (Fig. 7 right panel, dashed curve) produces only disordered aggregates. In fact a sharp peak centered at $P_2 = 0.48$ is evidenced. Parallel MD simulations carried out in a membrane-like environment exhibited a population of frames with a broad distribution of orientational order centered at $P_2 = 0.49$ (Fig. 7 right panel, solid curve). Notably, control simulations of NNFGAIL with free N- and C-termini, revealed an extended antiparallel β-sheet organization (data not shown) in agreement with results published elsewhere.[30]

This means that although the most populated system is a disordered one, a larger number of states characterized by a different orientational order are accessible during MD simulations. In other words, the system is able to explore a very large number of conformations. The affinity of the two types of aggregates for the membrane-like environment was established by plotting the number of frames as a function of their position along the Z direction of the lipid bilayer (Fig. 8).

It was evidenced that the trimeric aggregates of $hIAPP_{12–18}$ were mainly located at $Z = 0$ Å in the hydrocarbon core of the lipid bilayer. Conversely, the aggregates of $hIAPP_{21–27}$ are randomly distributed along the Z direction with a preferential position at the surface of the membrane ($Z = \pm 20$ Å), in agreement with the DSC results.

Discussion

Although it is widely acknowledged that amyloid deposits of IAPP are present in pancreatic tissues of the majority of type 2 Diabetes patients[53] the hypothesis that mature amyloid fibers may be the direct cause of cause β-cell death[54,55] has been more recently challenged by both *in vitro* and *in vivo* studies.[56–58]

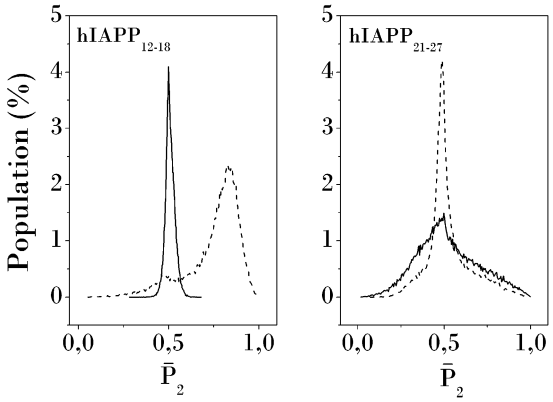

Fig. 7 Normalized populations *vs.* the total number of frames of $hIAPP_{12–18}$ (left panel) and $hIAPP_{21–27}$ (right panel) aggregates along the $\bar{P}_2$ order parameter calculated from MD simulations performed in an implicit membrane (solid lines) and water (dashed line). All simulations were performed at $T = 300$ K for 2 μs.

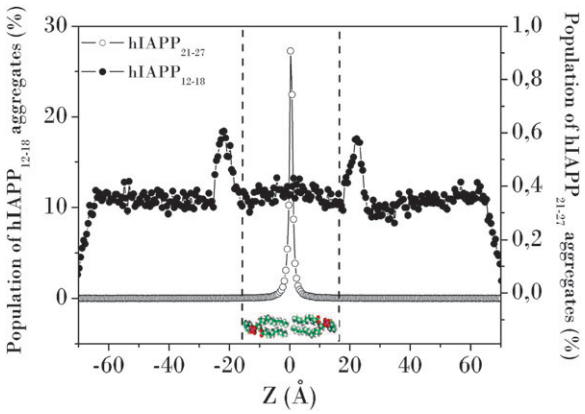

Fig. 8 One-dimensional distribution of populations of $hIAPP_{12–18}$ (filled circles) and $hIAPP_{21–27}$ (open circles) aggregates along the director (z-axis) of the DMPC lipid bilayer calculated from the analysis of the frames extracted from 2 μs implicit-membrane MD simulations at $T = 300$ K. Dashed lines represent the membrane/interface.

Peptide fragments of IAPP are thought to be useful in simplifying the analysis of the biophysical properties of IAPP by determining which residues are essential for both the biological and biophysical properties of the peptide. However, very few studies focused on the ability of specific IAPP sequences to interact with model membranes, are at present available in the literature.[59] In many cases these studies have been hampered by the poor solubility of these peptides, which has implicated the adoption of a sample handling protocol based on the dilution into the buffer from a peptide stock solution in organic solvents, *e.g.* hexafluoroisopropanol (HFIP) or dimethyl sulfoxide (DMSO).[60–62] Indeed, although these procedures allow to obtain highly reproducible starting conformeric states, ruling out any possible existence of pre-aggregated peptide assemblies before the experiments,[63] they should be adopted with caution in studies addressing peptide-induced changes in the thermotropic behavior of membranes, because organic solvents are known to affect the physico-chemical properties of lipid bilayers even at low

percentages.[64] Furthermore, if one wants to understand the role played by hydrophobic/electrostatic forces in driving lipid/peptide interactions, the rational choice of the model membrane is another critical factor: in fact it has been shown that negatively charged membranes may accelerate IAPP fibril growth and precipitation.[65] Unfortunately, in an attempt to mimic the physico-chemical features of natural cell membranes, a great number of studies were carried out to date by using a wide array of lipid mixtures with very different compositions, thus making a comparative analysis of the results unreliable. A specifically modified sample-handling protocol, coupled with the adoption of neutral lipid bilayers as model membranes, have allowed us to circumvent these experimental difficulties, evidencing that $hIAPP_{12–18}$ is not able either to modify the thermotropic behavior of membranes, or to induce their leakage. If coupled with the high fibrillogenicity observed for this peptide in water, these findings support the hypothesis that fibril growth is not an essential pre-requisite to induce membrane-damage, and reconcile with a view in which membrane-active oligomers are "off-pathway" by products that arise independently from fiber formation.[66–69] MD simulations have demonstrated that three replicas of $hIAPP_{12–18}$, if embedded in neutral model membranes, have a tendency to rapidly self-assemble to form a disordered aggregate. The affinity of this amorphous trimeric aggregate for the hydrophobic core of the membrane is very low and it is also observed that it preferentially lies on the surface of the membrane, in agreement with DSC experiments. Analogous MD simulations in water, have confirmed the high propensity of this peptide to self-assemble into ordered amyloid fibrils, as also evidenced by ThT fluorescence and Congo Red staining assays. Differently from $hIAPP_{12–18}$, the peptide $hIAPP_{21–27}$ did not assemble into amyloid fibrils in water, but exhibited a noticeable ability to perturb the thermotropic behavior of DMPC LUVs, which was associated to membrane leakage as evidenced by DSC and dye-release experiments. MD simulations of the aggregation process of $hIAPP_{21–27}$ in water and in a membrane-like environment confirmed the poor tendency of this peptide to self-assemble into highly ordered structures in both the environments. In particular, the trimeric assembly of $hIAPP_{21–27}$ if immersed in membrane-like structures exhibited a preferential affinity for the hydrocarbon core of the bilayer. There, it assumes a poorly ordered structure, but, differently from what was observed for $hIAPP_{12–18}$, the distribution of the populations along the order parameter P_2 is broader, although centered at $P_2 = 0.48$. These findings suggest that the system, especially in the membrane environment, is able to sample a wider conformational space exhibiting a great conformational variability, as shown in Fig. 9, where some representative snapshots describing these results are reported.

The poor amyloidogenicity here observed for $hIAPP_{21–27}$ although confirming previously reported data[38] is in apparent contrast with several pieces of data reporting the hIAPP region localized on residues 20–29 as the most critical domain for hIAPP amyloid formation.[30,31,33,70,71] Several reasons may explain these differences: first, differently from the present work, most of those studies have used peptides with unblocked N- and C-termini whose electrostatic charges are thought to deeply influence the aggregation properties of the peptide. Second, recent data concerning the atomic structure obtained from microcrystals of the segment NNFGAIL reveals an unusual packing of β-sheet layers, which contain a bend facilitated by the central glycine, allowing a tight (3 Å) main-chain interface between F, G and A of opposing sheets.[72] Furthermore, the shorter peptide segments NFGAIL and FGAIL were shown to aggregate into completely different fibrillar assemblies, thus highlighting the significant morphological variability that occurs in this region.[29] Given that a thorough characterization of amyloid oligomers in the presence of lipid vesicles appears to be experimentally challenging, our results provide significant data supporting the hypothesis that fibril growth and peptide-induced membrane damage are two distinct processes whose molecular determinants are located in different regions of the hIAPP sequence.[73]

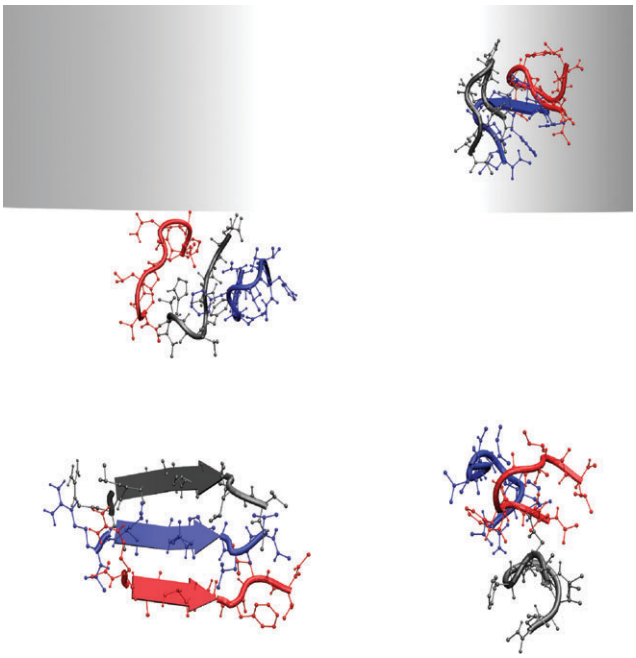

Fig. 9 Snapshot of $hIAPP_{12–18}$ and $hIAPP_{21–27}$ aggregates in water (bottom) and in membrane-like environments (top, grey zone represents the membrane environment).

Acknowledgements

This work was financially supported by Università degli Studi di Catania and CNR (grant RSTL no 620). Some of the molecular simulations were performed by using the computational resources of CASPUR (AMD Opteron 50 CPU Linux Clusters).

Notes and references

1 J. D. Sipe, *Crit. Rev. Clin. Lab. Sci.*, 1994, **31**, 325–354.
2 A. Lorenzo, B. Razzaboni, G. C. Weir and B. A. Yankner, *Nature*, 1994, **368**, 756–760.
3 J. D. Harper and P. T. Lansbury, *Annu. Rev. Biochem.*, 1997, **66**, 385–407.
4 S. B. Prusiner, M. R. Scott, S. J. DeArmond and F. E. Cohen, *Cell*, 1998, **93**, 337–348.
5 A. Clark, G. J. Cooper, C. E. Lewis, J. F. Morris, A. C. Willis, K. B. Reid and R. C. Turner, *Lancet*, 1987, **330**, 231–234.

6 P. Westermark, E. Wilander, G. T. Westermark and K. H. Johnson, *Diabetologia*, 1987, **30**, 887–892.
7 C. Betsholtz, V. Svensson, F. Rorsman, U. Engstrom, G. T. Westermark, E. Wilander, K. Johnson and P. Westermark, *Exp. Cell Res.*, 1989, **183**, 484–493.
8 C. E. Higham, E. T. Jaikaran, P. E. Fraser, M. Gross and A. Clark, *FEBS Lett.*, 2000, **470**, 55–60.
9 R. Kayed, J. Bernhagen, N. Greenfield, K. Sweimeh, H. Brunner, W. Voelter and A. Kapurniotu, *J. Mol. Biol.*, 1999, **287**, 781–796.
10 J. Janson, R. H. Ashley, D. Harrison, S. Mcintyre and P. C. Butler, *Diabetes*, 1999, **48**, 491–498.
11 T. A. Mirzabekov, M. Lin and B. L. Kagan, *J. Biol. Chem.*, 1996, **271**, 1988–1992.
12 M. Anguiano, J. N. Richard and P. T. Lansbury, Jr, *Biochemistry*, 2002, **41**, 11338–11343.
13 B. Konarkowska, J. F. Aitken, J. Kistler, S. P. Zhang and G. J. S. Cooper, *FEBS J.*, 2006, **273**, 3614–3624.
14 P. E. S. Smith, J. R. Brender and A. Ramamoorthy, *J. Am. Chem. Soc.*, 2009, **131**, 4470–4478.
15 R. P. R. Nanga, J. R. Brender, J. Xu, K. Hartman, V. Subramanian and A. Ramamoorthy, *J. Am. Chem. Soc.*, 2009, **131**, 8252–8261.
16 J. R. Brender, K. Hartman, K. R. Reid, R. T. Kennedy and A. Ramamoorthy, *Biochemistry*, 2008, **47**, 12680–12688.
17 A. Demuro, E. Mina, R. Kayed, S. C. Milton, I. Parker and C. G. Glabe, *J. Biol. Chem.*, 2005, **280**, 17294–17300.
18 H. A. Lashuel and P. T. Lansbury, *Q. Rev. Biophys.*, 2006, **39**, 167–201.
19 L. O. Tjernberg, C. Lilliehook, D. J. E. Callaway, J. Naslund, S. Hahne, J. Thyberg, L. Terenius and C. Nordstedt, *J. Biol. Chem.*, 1997, **272**, 12601–12605.
20 L. A. Scrocchi, Y. Chen, S. Waschuk, F. Wang, S. Cheung, A. A. Darabie, J. McLaurin and P. E. Fraser, *J. Mol. Biol.*, 2002, **318**, 697–706.
21 A. Kapurniotu, A. Schmauder and K. Tenidis, *J. Mol. Biol.*, 2002, **315**, 339–350.
22 C. Betsholtz, L. Christmanson, U. Engstrom, F. Rorsman, K. Jordan, T. D. O'Brien, M. Murtaugh, K. H. Johnson and P. Westermark, *Diabetes*, 1990, **39**, 118–122.
23 G. Glenner, E. D. Eanes and C. A. Wiley, *Biochem. Biophys. Res. Commun.*, 1988, **155**, 608–614.
24 P. Westermark, U. Engstrom, K. H. Johnson, G. T. Westermark and C. Betsholtz, *Proc. Natl. Acad. Sci. U. S. A.*, 1990, **87**, 5036–5040.
25 M. D. George, G. Glenner, E. D. Eanes and M. D. Clayton, *Protein*, 1988, **155**, 608–614.
26 A. Mascioni, F. Porcelli, U. Ilangovan, A. Ramamoorthy and G. Veglia, *Biopolymers*, 2003, **69**, 29–41.
27 U. Ilangovan and A. Ramamoorthy, *Biopolymers*, 1998, **45**, 9–20.
28 K. Tenidis, M. Waldner, J. Bernhagen, W. Fischle, M. Bergmann and M. Weber, *J. Mol. Biol.*, 2000, **295**, 1055–1071.
29 R. C. Elgersma, G. e. Mulder, J. A. W. Krujteer, G. Psthuma, D. T. S. Riskers and R. M. J. Liskamp, *Bioorg. Med. Chem. Lett.*, 2007, **17**, 1837–1842.
30 J. T. Nielsen, M. Bjerring, M. D. Jeppesen, R. O. Pedersen, J. M. Pedersen, K. L. Hein, T. Vosegaard, T. Skrydstrup, D. E. Otzen and N. C. Nielsen, *Angew. Chem., Int. Ed.*, 2009, **48**, 2118–2121.
31 M. R. Nilsson and D. P. Raleigh, *J. Mol. Biol.*, 1999, **294**, 1375–1385.
32 E. T. Jaikaran, C. E. Higham, L. C. Serpell, J. Zurdo, M. Gross, A. Clark and P. E. Fraser, *J. Mol. Biol.*, 2001, **308**, 515–525.
33 C. Goldsbury, K. Goldie, J. Pellaud, J. Seeling, P. Frey, S. A. Muller, J. Kistler, G. J. S. Cooper and U. Aebi, *J. Struct. Biol.*, 2000, **130**, 352–362.
34 M. Tatarek-Nossol, L. M. Yan, A. Shmauder, K. Tenidis, G. Westermark and A. Kapurniotu, *Chem. Biol.*, 2005, **12**, 797–809.
35 L. A. Scrocchi, K. Ha, Y. Chen, L. Wu, F. Wang and P. E. Fraser, *J. Struct. Biol.*, 2003, **141**, 218–227.
36 K. F. DuBay, A. P. Pawar, F. Chiti, J. Zurdo, C. M. Dobson and M. Vendruscolo, *J. Mol. Biol.*, 2004, **341**, 1317–1326.
37 A. M. Fernandez-Escamilla, F. Rousseau, J. Schymkowitz and L. Serrano, *Nat. Biotechnol.*, 2004, **22**, 1302–1316.
38 M. Cecchini, R. Curcio, M. Pappalardo, R. Melki and A. Caflisch, *J. Mol. Biol.*, 2006, **357**, 1306–1321.
39 N. V. Buchete, R. Tycko and G. Hummer, *J. Mol. Biol.*, 2005, **353**, 804–821.
40 M. F. M. Sciacca, M. Pappalardo, D. Milardi, D. Grasso and C. La Rosa, *Arch. Biochem. Biophys.*, 2008, **477**, 291–298.
41 M. Cecchini, F. Rao, M. Seeber and A. Caflisch, *J. Chem. Phys.*, 2004, **121**, 10748–56.
42 D. Grasso, D. Milardi, C. La Rosa and E. Rizzarelli, *New J. Chem.*, 2001, **25**, 1543–1548.
43 R. C. MacDonald, R. I. MacDonald, B. P. Menco, K. Takeshita, N. K. Subarrao and L. Hu, *Biochim. Biophys. Acta, Biomembr.*, 1991, **1061**, 297–303.
44 B. R. Brooks, R. E. Bruccoleri, B. D. Olafson, D. J. States, S. Swaminathan and M. Karplus, *J. Comput. Chem.*, 1983, **4**, 187–217.
45 E. Neria, S. Fischer and M. Karplus, *J. Chem. Phys.*, 1996, **105**, 1902–1921.
46 J. Gsponer, U. Habertur and A. Caflisch, *Proc. Natl. Acad. Sci. U. S. A.*, 2003, **100**, 5154–5159.
47 T. Lazaridis and M. Karplus, *Proteins: Struct., Funct., Genet.*, 1999, **35**, 133–152.
48 T. Lazaridis and M. Karplus, *J. Mol. Biol.*, 1999, **288**, 477–487.
49 T. Lazaridis, *Proteins: Struct., Funct., Genet.*, 2003, **52**, 176–192.
50 K. A. Henzler-Wildman, G. V. Martinez, M. F. Brown and A. Ramamoorthy, *Biochemistry*, 2004, **43**, 8459–8469.
51 D. Grasso, G. Grasso, V. Guantieri, G. Impellizzeri, C. La Rosa, D. Milardi, G. Micera, K. Osz, G. Pappalardo, E. Rizzarelli, D. Sanna and I. Sovago, *Chem.–Eur. J.*, 2006, **12**, 537–547.
52 R. P. R. Nanga, J. R. Brender, J. Xu, G. Veglia and A. Ramamoorthy, *Biochemistry*, 2008, **47**, 12689–12697.
53 A. Clark and M. R. Nilsson, *Diabetologia*, 2004, **47**, 157–169.
54 J. W. M. Hoppener and C. J. M. Lips, *Int. J. Biochem. Cell Biol.*, 2006, **38**, 726–736.
55 A. Lorenzo and B. A. Yankner, *Neurobiol. Alzheimer's Dis.*, 1996, **777**, 89–95.
56 R. L. Hull, Z. P. Shen, M. R. Watts, K. Kodama, D. B. Carr, K. M. Utzschneider, S. Zraika, F. Wang and S. E. Kahn, *Diabetes*, 2005, **54**, 2235–2244.
57 Y. Tasaka, F. Nakaya, H. Matsumoto, Y. Iwamoto and Y. Omori, *Pancreas*, 1995, **11**, 303–308.
58 E. T. Bell, *Am. J. Pathol.*, 1959, **35**, 801–805.
59 G. Pappalardo, D. Milardi, A. Magrí, F. Attanasio, G. Impellizzeri, C. La Rosa, D. Grasso and E. Rizzarelli, *Chem.–Eur. J.*, 2007, **13**, 10204–10215.
60 M. F. M. Engel, H. A. Yigittop, R. C. Elgersma, D. T. S. Rijkers, R. M. J. Liskamp, B. De Kruijff, J. W. M. Höppener and J. A. Killian, *J. Mol. Biol.*, 2006, **356**, 783–789.
61 M. A. Kiselev, T. Gutberlet, P. Lesieur, T. Hauss, M. Ollivon and R. H. H. Neubert, *Chem. Phys. Lipids*, 2005, **133**, 181–193.
62 J. L. Larson and A. D. Miranker, *J. Mol. Biol.*, 2004, **335**, 221–231.
63 N. Hirota, K. Mizuno and Y. Goto, *J. Mol. Biol.*, 1998, **275**, 365–378.
64 R. Notman, M. Noro, B. O'Malley and J. Anwar, *J. Am. Chem. Soc.*, 2006, **128**, 13982–13983.
65 A. D. Miranker, *Methods Mol. Biol.*, 2005, **299**, 185–194.
66 J. J. Meier, R. Kayed, C. Y. Lin, T. Gurlo, L. Haataja, S. Jayasinghe, R. Langen, C. G. Glabe and P. C. Butler, *Am. J. Physiol.*, 2006, **291**, 1317–1324.
67 M. Necula, L. Breydo, S. Milton, R. Kayed, W. E. Van der Veer, P. Tone and C. G. Glabe, *Biochemistry*, 2007, **46**, 8850–8860.
68 M. Necula, R. Kayed, S. Milton and C. G. Glabe, *J. Biol. Chem.*, 2007, **282**, 10311–10324.
69 J. W. Hoppener, M. G. Nieuwenhuis, T. M. Vroom and C. J. Lips, *N. Engl. J. Med.*, 2000, **144**, 1995–2000.
70 J. R. Brender, U. H. N. Durr, D. Heyl, M. B. Budarapu and A. Ramamoorthy, *Biochim. Biophys. Acta, Biomembr.*, 2007, **1768**, 2026–1029.
71 A. M. Ruschak and A. D. Miranker, *Proc. Natl. Acad. Sci. U. S. A.*, 2007, **104**, 12341–12346.
72 J. J. W. Wiltzius, S. A. Sievers, M. R. Saway, D. Cascio, D. Popov, C. Riekel and D. Eisenberg, *Protein Sci.*, 2008, **17**, 1467–1474.
73 J. R. Brender, E. L. Lee, M. A. Cavitt, A. Gafni, D. G. Steel and A. Ramamoorthy, *J. Am. Chem. Soc.*, 2008, **130**, 6424–6429.